
STRUCTURE TO PROPERTY: CHEMICAL ELEMENT EMBEDDINGS AND A DEEP LEARNING APPROACH FOR ACCURATE PREDICTION OF CHEMICAL PROPERTIES

A PREPRINT

✉ Shokirbek Shermukhamedov^{1,*}, Dilorom Mamurjonova², Michael Probst^{1,3}

¹Institute of Ion Physics and Applied Physics, University of Innsbruck, 6020 Innsbruck, Austria

²Tashkent Chemical Technological Institute, 100011 Tashkent, Uzbekistan

³School of Molecular Science and Engineering, Vidyasirimedhi Institute of Science and Technology, 21201 Rayong, Thailand

**Author to whom any correspondence should be addressed.*

E-mail: shokirbek.shermukhamedov@uibk.ac.at

August 20, 2024

ABSTRACT

We introduce the eEmBERT model for chemical classification tasks. It is based on deep learning techniques, such as a multilayer encoder architecture. We demonstrate the opportunities offered by our approach on sets of organic, inorganic and crystalline compounds. In particular, we developed and tested the model using the *Matbench* and *MoleculeNet* benchmarks, which include crystal properties and drug design-related benchmarks. We also conduct an analysis of vector representations of chemical compounds, shedding light on the underlying patterns in structural data. Our model exhibits exceptional predictive capabilities and proves universally applicable to molecular and material datasets. For instance, on the Tox21 dataset, we achieved an average precision of 96%, surpassing the previously best result by 10%.

Keywords Machine Learning, Transformer, BERT, MoleculeNet, Matbench

1 Introduction

Due to their effectiveness in fitting experimental data and predicting material properties, machine learning models have found extensive applications in research on batteries Ng et al. [2020], Liu et al. [2020], supercapacitors Sawant et al. [2023], thermoelectric Iwasaki et al. [2019], and photoelectric Akhter et al. [2019] devices, catalysts Toyao et al. [2020], and in drug design Vamathevan et al. [2019]. In a 'second wave', deep learning models (DLMs) have exhibited remarkable potential in advancing the field of chemical applications. Word2vec Mikolov et al. [2013] DLMs have been used for processing textual chemical data extracted from academic articles. By representing chemical formulas as embeddings or vectors, non-obvious connections between compounds and chemical properties can be discovered. For instance, the mat2vec Tshitoyan et al. [2019] NLP model was able to predict materials with good thermoelectric properties even when these materials and their properties were not explicitly named in the original papers. Other NLP-inspired models such as Bag of Bonds Hansen et al. [2015], mol2vec Jaeger et al. [2018], smiles2vec Goh et al. [2018], SPvec Zhang et al. [2020a] have used unsupervised machine learning and have been applied to chemical compound classification tasks, achieving remarkable results. These models hold immense potential for accelerating the discovery and design of materials with tailored properties.

In this regard, the type of input data is crucial for ML models. In chemistry, this could be chemical text data like in mat2vec or structural data. Chemical texts make it possible to use reference information about a compound Stanev et al.

[2018] such as molecular weight, melting point, crystallization temperature, and element composition. These types of inputs can in turn be used by general deep learning models with ELMO, BERT, and GPT-4 being the most famous examples. However, such models cannot directly capture 3D information from structural files.

One of the most common types of input data used for ML-based approaches is structural representation, which provides valuable information about the atomic environment of a given material. However, text-based data does not normally capture important structural features such as interatomic distances. Structural information is crucial for predicting material properties, as it is key to all pertinent physical and chemical characteristics. This can be understood in the same sense as the Born-Oppenheimer approximation, which in short states that atomic coordinates (and from them the potential energy) are all that is needed in chemistry. The challenge of linking structural information to material properties is commonly referred to as the "structure to property" task. Overcoming this challenge has the potential to greatly enhance our ability to predict and design novel materials with desired properties.

Structure can be translated into property by graph neural networks (GNN) or high-dimensional neural networks (HDNN) formalisms. GNNs transform graphs of molecules (or compounds) into node and edge embeddings, which can then be used for state-of-the-art tasks Chen et al. [2019], Kong et al. [2022], Gori et al. [2005], Zhang et al. [2020b], Shui and Karypis [2020], Fung et al. [2021], Xie and Grossman [2018], Guo et al. [2021]. GNNs are efficiently applied for both chemical classification and regression tasks. However, as the size and complexity of molecular graphs increase, the computational requirements for GNNs also grow. Handling large graphs with many atoms or intricate structures can pose scalability challenges both in terms of memory usage and computer time. HDNNs based on converting Cartesian coordinates of atoms to continuous representations utilize techniques such as smooth overlap of atomic positions (SOAP) Bartók et al. [2013], many-body tensor representation (MBTR) Huo and Rupp [2022], or atomic centered symmetry functions (ACSF) Behler [2021] to achieve the same goal. Message passing neural networks (MPNN) are a subgroup of HDNN that employ atomic positions and nuclear charges as input. The PhysNet Unke and Meuwly [2019] model serves as a typical example. In this model, atomic embedding encodes the atomic identifier into vector arrays, which are first initialized randomly and optimized during training.

HDNNs demonstrate excellent performance on regression tasks. However, in classification tasks, GNNs dominate. Moreover, a disadvantage of HDNNs is their susceptibility to overfitting and their computational complexity. As the dimensionality increases, the possibility of overfitting rises due to the larger number of parameters, and the training time also increases.

Despite the increasing use of deep learning in computational chemistry, many aspects of NLP models have yet to be fully explored. One of them is the attention mechanism Vaswani et al. [2023], which allows the model to focus on specific parts of the input data when making predictions. It works by assigning different levels of importance or attention to different elements in the input sequence. The attention mechanism has been previously used in graph neural networks Louis et al. [2020]. Additionally, the transformer approach, commonly known for its successful application in chemical GNNs, has not been fully extensively applied to HDNNs. The transformer consists of two distinct components: an encoder responsible for processing the input data and a decoder responsible for generating task-related predictions. In this paper, we introduce a new deep learning model for chemical compounds that utilizes the encoder part of the Transformer architecture. Specifically, our model incorporates local attention layers to capture properties of local atomic environments and then utilizes a global attention layer to make weighted aggregations of these atomic environment vectors to create a global representation of the entire chemical structure. From its components, we call this model 'eEmBERT' (**e**lement **E**mbdings and **B**idirectional **E**ncoder **R**epresentations from **T**ransformers).

In summary, the main aspects of our work are:

- We use a transformer mechanism for binary and multilabel classification based on structural information.
- Our model is flexible, fast, and can be easily adapted to different types of datasets.
- Benchmarks show the state-of-the-art performance of our model for a variety of material property prediction problems, both involving organic and inorganic compounds.

2 Methods

As input to the neural network (NN), we use atomic pair distribution functions (PDFs) and the atom types that compose the compounds. The PDF represents the probability of finding an atom inside a sphere with a radius r_{cut} centered at a selected atom Billinge [2019]. To prepare the training data, we calculate PDFs employing the ASE library Hjorth Larsen et al. [2017] with a cutoff radius of 10 Å Shermukhamedov et al. [2024]. The second input for the NN consists of element embedding vectors. To achieve this, all elements in all compounds are mapped to integers (typically using the nuclear charge), creating an elemental vocabulary of size $V_{\text{size}} = 101$. These embeddings are then passed to the

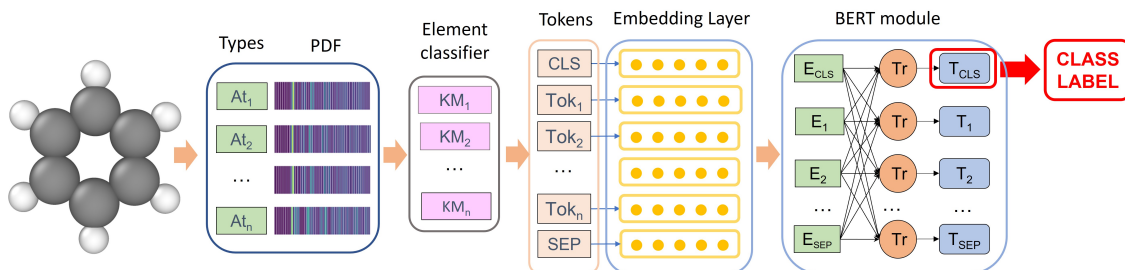


Figure 1: **eEmBERT model architecture.** The initial step involves computing the pair distribution function for each element based on atom positions within the chemical compound. This information is then passed through the classifier model. Subsequently, the resulting sub-elements are converted into tokens, with additional tokens incorporated before input into the BERT module. The [CLS] token output vector from BERT is used for the classification task.

BERT module. BERT is a deep learning architecture originally designed for natural language processing (NLP) tasks. It employs a bidirectional transformer encoder to capture word context in sentences, allowing it to generate accurate text representations. BERT employs masked language modeling (MLM), where some tokens in a sentence are masked or replaced with a [MASK] token, and the model is trained to predict the original word based on the surrounding context.

2.1 Model architecture

Our model architecture is illustrated in Fig. 1. It can use various combinations of embedding sizes, encoder layers, and attention heads. In chemical applications, the atomic composition of a compound can be equated to a sentence, with individual atoms serving as constituent tokens. Leveraging this analogy, we introduce four new tokens to the vocabulary: [MASK] for MLM, [UNK] for unseen tokens, [CLS] for classification, and [SEP] for separating two compounds. In standard BERT models positional embeddings play an important role by encoding the order of tokens in a sequence, which allows the model to capture sequential relationships between tokens. Since the Transformer approach is inherently permutation-invariant – treating different permutations of the same input sequence identically – there is no explicit encoding of token order. As well, in chemical compounds, the order of atoms does not affect the properties of the entire compound. Correspondingly, in our implementation, positional embeddings are intentionally omitted to preserve permutation invariance. In chemical compounds, elements may exhibit varying oxidation states or formal charges, indicating the relative electron loss or gain during reactions. The interactions between these elements are non-uniform and follow specific patterns based on their neighboring atoms. For inorganic substances, these interactions typically appear as ionic interactions, signified by the oxidation state, while in organic substances, covalent bonding is prevalent.

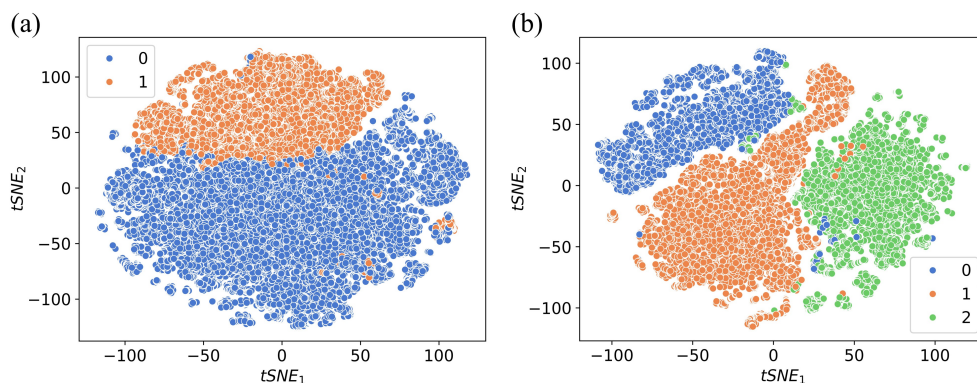


Figure 2: **Sub-element classification:** t-SNE Plots for Li (a) and Mg (b) atoms extracted from atomic PDFs of COD database.

To establish a universal criterion for categorizing these interactions, we divided the elements in our training dataset into “sub-elements” based on the local environment of atoms in compounds. We use the PDF and the oxidation state of each element to determine the number of possible sub-elements. It is crucial to note that information about the specific interaction type in molecular structures is often missing, which can lead to algorithmic errors. Recognizing that bond

length contains information about interactions, we used unsupervised clustering to categorize elements. This approach is similar to the methods used manually in the development of classical force fields Damm et al. [1997]. We evaluated several algorithms and ultimately selected the k-means (Km) algorithm due to its speed and simplicity. For fitting, we utilized structures from the Crystallography Open Database (COD) Gražulis et al. [2009, 2012]. Detailed information is provided in Appendix A. To illustrate the workings of our approach, we present examples of sub-element classifications for lithium (Li) and magnesium (Mg) atoms in Fig. 2. In these examples, Li and Mg atoms are classified into two and three groups, respectively. These t-SNE (t-distributed stochastic neighbor embedding) reductions of atomic PDFs provide a visualization of the principles behind atom division into sub-elements. We fitted an individual model for each element in our dataset, resulting in a total of 96 models. The final size of the dictionary, including sub-element tokens, was $V_{size} = 565$. Examples of such differentiation are presented in Fig. 3.

2.2 Datasets

We trained our eEmBERT model to perform various classification tasks. To do this, we used the [CLS] token and added an additional layer to the BERT module with the same number of neurons as there are classes in the dataset. Our first task involved using the Materials Project (MP) metallicity dataset to predict the metallicity of materials based on structural information Jain et al. [2013], Ong et al. [2015]. Next, we employed a portion of the datasets gathered for the CegaNN model Banik et al. [2023]. This led us to undertake a classification task known as the Liquid-Amorphous (LA) task, which revolves around distinguishing between liquid and amorphous phases of silicon (Si). The LA dataset comprises 2,400 Si structures, evenly divided between amorphous and liquid phases (50% each). Importantly, these Si structures lack symmetry and differ solely in terms of density and coordination number. In addition to these

tasks, we evaluated the eEmBERT model’s ability to classify material polymorphs across different dimensionalities, specifically clusters (0D), sheets (2D), and bulk structures (3D). Carbon, with its wide range of allotropes spanning these dimensionalities, served as an excellent system for assessing the efficiency of our network model in dimensionality classification (DIM task). The DIM dataset contained 1,827 configurations. Finally, we ventured into characterizing the space group of crystal structures, encompassing a total of 10,517 crystal structures distributed among eight distinct space groups (SG task) Ziletti et al. [2018]. Expanding beyond inorganic material datasets, we incorporated organic compounds, which greatly outnumber their inorganic counterparts. This expansion encompasses an extended range of properties, including biochemical and pharmaceutical aspects. To rigorously validate our model, we turned to benchmark datasets from MoleculeNet Wu et al. [2018], specifically BBBP (Blood-Brain Barrier Penetration), ClinTox (Clinical Toxicity), BACE (β -Secretase), SIDER (Side Effect Resource) Kuhn et al. [2016], and Tox21. Notably, the Tox21 and SIDER datasets encompass 12 and 27 individual tasks, respectively, each corresponding to specific toxicity predictions. These datasets cover a diverse array of chemical compounds and provide a comprehensive assessment of our model’s predictive performance for binary properties or activities associated with organic molecules. In this context, a positive instance signifies that a molecule possesses a specific property, while a negative instance indicates its absence. The MoleculeNet dataset primarily comprises organic molecules represented in Simplified Molecular Input Line Entry System (SMILES) format. For purposes of analysis, we converted these SMILES formulas into the standard XYZ format using the Open Babel software O’Boyle et al. [2011] and the RDKit package RDK. To evaluate our model’s performance, we employed the "Receiver Operating Characteristic - Area Under the Curve" (ROC-AUC) metric, a common measure for assessing binary classification quality. ROC-AUC quantifies the model’s ability to differentiate between positive and negative classes based on predicted probabilities.

2.3 Training procedure

In the following sections, we will present the results of prediction models with specific parameters, including an embedding size of 32, 2 attention heads, and 2 layers. These parameter choices have been identified as optimal across

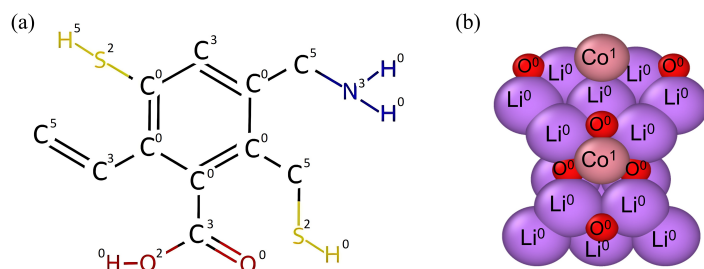


Figure 3: **Examples illustrating the division of elements into sub-elements based on their environment:** a hypothetical organic compound (a) and Li_8CoO_6 (b) crystal with ID mp-27920. The numbers at the top right of elements correspond to sub-element indexes.

all datasets considered in this study. We explored two model versions, V0 (where the Km block is omitted) and V1, as discussed previously. These models were implemented using Keras Chollet et al. [2015] and were trained with eight-fold splitting. This procedure is responsible for the splitting of the dataset and the initiation of model weights. We split the datasets into three subsets: the training set, the validation set, and the test set, with an 80:10:10 ratio. We employed the categorical crossentropy loss function with the Adam optimizer, setting the learning rate at 0.001. The batch size was set to 128 for the MP task and 32 for the other datasets. The number of epochs was two and four times the batch size, respectively.

3 Results

The ROC-AUC values reported in Table 1 represent averages over all test set prediction values. The table clearly demonstrates that the prediction efficiency improves as the number of tokens increases, particularly for inorganic compounds. In the LA task, using single-element inputs results in only 50% accuracy, which is comparable to random guessing. However, incorporating sub-elements significantly enhances the performance, leading to an impressive ROC-AUC of 0.983. Our approach also demonstrates improved scores across other datasets. In the subsequent sections, we will delve into each dataset, from Matbench to Tox21, and examine the eEmBERT-V1 model in more detail, providing comprehensive insights into the predictions.

Table 1: Performance of eEmBERT models applied to datasets used in this work. A **bold** font indicates the best performance, an underline represents the second-best performance, and the last column presents previous results obtained from other models. V0 represents models that use chemical element embeddings, while V1 uses sub-element embeddings as input for the BERT module.

Benchmark	V0	V1	Best
MP metallicity	0.961	0.965	0.950 Chen and Ong [2021]
SG	0.945	<u>0.952</u>	1.000 Banik et al. [2023]
LA	0.500	<u>0.983</u>	1.000 Banik et al. [2023]
DIM	0.866	<u>0.958</u>	1.000 Banik et al. [2023]
BACE	0.732	<u>0.789</u>	0.888 Li et al. [2022]
BBBP	0.903	<u>0.909</u>	0.932 Li et al. [2022]
ClinTox	0.962	<u>0.959</u>	0.948 Li et al. [2021]
HIV	0.982	<u>0.972</u>	0.776 Baek et al. [2021]
SIDER	0.778	<u>0.773</u>	0.659 Li et al. [2022]
Tox21	<u>0.965</u>	0.967	0.860 Li et al. [2021]

3.1 MP metallicity

In this task, the objective is to predict whether a material is metallic or non-metallic, a property initially determined by electronic structure calculations. Fig. 4a illustrates the confusion matrix and presents the performance of the eEmBERT-V1 model in classifying MP metallicity. The dataset for this task comprises 106,113 samples of training structures and 21,222 samples of test structures. Our trained model achieves a binary accuracy of approximately 0.910 and an AUC of 0.965 on the test set. In Fig. 4b, the t-SNE plot shows the embeddings of the entire reference dataset, categorized by labels. A smooth differentiation among labels within the feature space is revealed. Fig. 4c illustrates how the reference dataset is classified by our model. The classification layer creates a clear separation in the feature space, in contrast to the diffuse boundary in the reference dataset. Primary errors are located at the boundary, where the model sometimes struggles to effectively capture diffusive behavior. The metallicity prediction task highlights eEmBERT’s remarkable capability to characterize these binary properties of crystals. The results exceed the capabilities of previously published models, including those of GNNs.

3.2 LA, DIM and SG datasets

This section presents the results from benchmarks conducted on the CegaNN dataset, with an initial focus on the LA classification task. Figs. 5a and 5b show the embedding representation of Si structures based on their labels, reduced through the t-SNE algorithm. Our model effectively separates the structures into distinct clusters, with two clusters clearly corresponding to their respective classes. However, one cluster exhibits intermixing of structures, which challenges accurate recognition by the model. The confusion matrices shown in Fig. 5c-e provide insights into the performance of the eEmBERT-V1 model across the LA, DIM, and SG datasets. The model achieves a high ROC-AUC

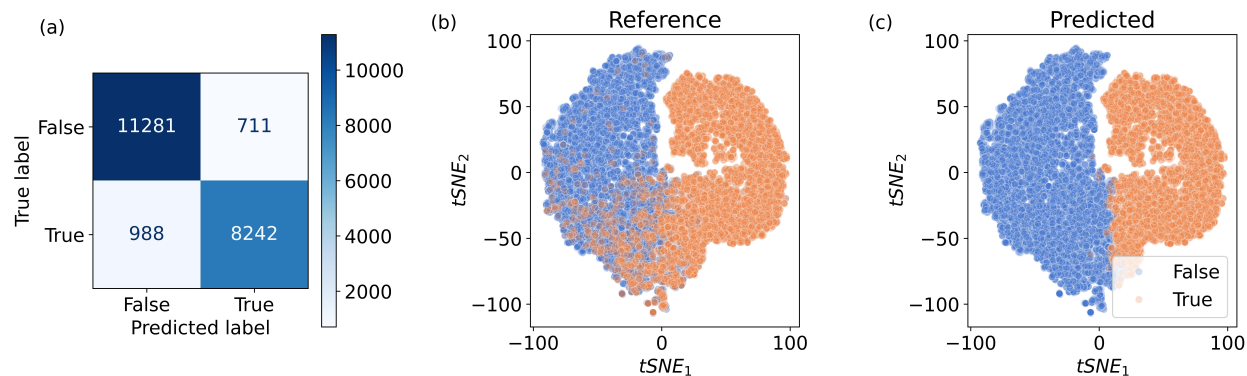


Figure 4: **MP metallicity**: Confusion matrix (a) and visualization of [CLS] token embeddings for the MP metallicity dataset for the reference (b) and predicted (c) datasets: blue circles denote negative labels (not metal) and orange dots represent positive labels (metal).

of approximately 0.958 on the DIM task’s test set and a slightly higher value of 0.968 on the SG dataset. These confusion matrices illustrate the model’s ability to identify and categorize each structure accurately. It is worth noting that the model faces challenges in distinguishing the bcc (229) structure from others in the SG dataset. This challenge arises from the structural similarities between the bcc structure and others, resulting in identical geometrical representations unless the orientational order of the particles is considered. While the CegaNN model achieves approximately 100% accuracy in this benchmark, our model approaches this level of performance, also exhibiting strengths in versatility, speed, and simplicity.

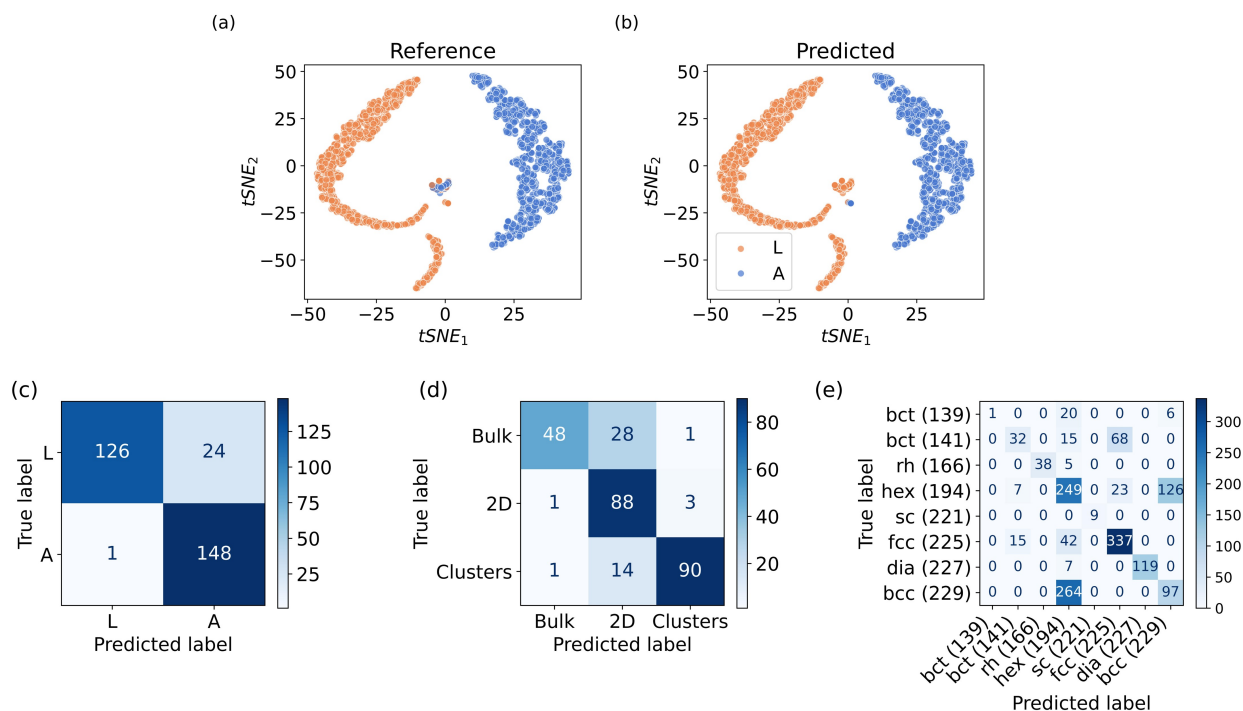


Figure 5: **Classification task of inorganic compounds**. Top row: Visualization of [CLS] Token Embeddings for the LA Dataset: a) reference labels and b) predicted labels. The embeddings are represented using blue circles for liquid phase labels and orange dots for amorphous labels. Bottom row: Confusion matrix analysis of the LA (c), DIM (d), and SG (e) datasets.

3.3 Tox21 dataset

The Tox21 dataset is a collection of chemical compounds evaluated for their toxicity against 12 biological targets. With over 8,000 compounds, it serves as a valuable resource for predicting the toxicity and potential adverse effects of various chemical compounds. Our model, trained on the Tox21 dataset, demonstrated impressive performance, achieving an average AUC of 0.96 across all 12 toxicity prediction tasks Wu et al. [2018]. The results of these individual tasks are presented in Table 2, enabling a comprehensive evaluation of the model’s performance on each toxicity task.

Comparing our results with those of the Meta-Molecular GNN (MMGNN) model Guo et al. [2021] highlights the significant advantages of our approach. Fig. 6 shows the confusion matrix of the test set and the t-SNE projection representing the features of the sr-mmp task in the Tox21 dataset. As shown, our model predicts distinct patterns in the t-SNE projections, with each label value occupying a specific region (Fig. 6b). The molecular embedding visualizations are also available in the MMGNN model report for the sr-mmp task Guo et al. [2021]. In contrast, our feature space exhibits more structure, with positive values being less dispersed across all compounds. Our model primarily has a few points that are significantly distant from the positive value region. Both eEmBERT models successfully identify the boundary between these two classes and make predictions (Fig. 6). Errors primarily arise from diffuse boundary regions and points located far from the true cluster. This observation holds true for all Tox21 tasks. Similarly, prediction analysis for the BACE, BBBP, ClinTox, HIV, and SIDER datasets is detailed in Appendix B.

Table 2: ROC-AUC performance of different tasks from the Tox21 dataset. MMGNN denotes the prior top-performing results Guo et al. [2021]. Averaged score across all tasks showed in Table 1.

Model	nr-ahr	nr-ar-lbd	nr-arom	nr-ar	nr-er-lbd	nr-er
V0	0.955	0.987	0.980	0.983	0.978	0.932
V1	0.961	0.989	0.979	0.982	0.978	0.935
MMGNN	-	-	-	-	-	-
Model	nr-ppar-gamma	sr-are	sr-atad5	sr-hse	sr-mmp	sr-p53
V0	0.988	0.913	0.985	0.974	0.938	0.972
V1	0.986	0.913	0.983	0.974	0.946	0.973
MMGNN	-	-	-	0.748	0.804	0.790

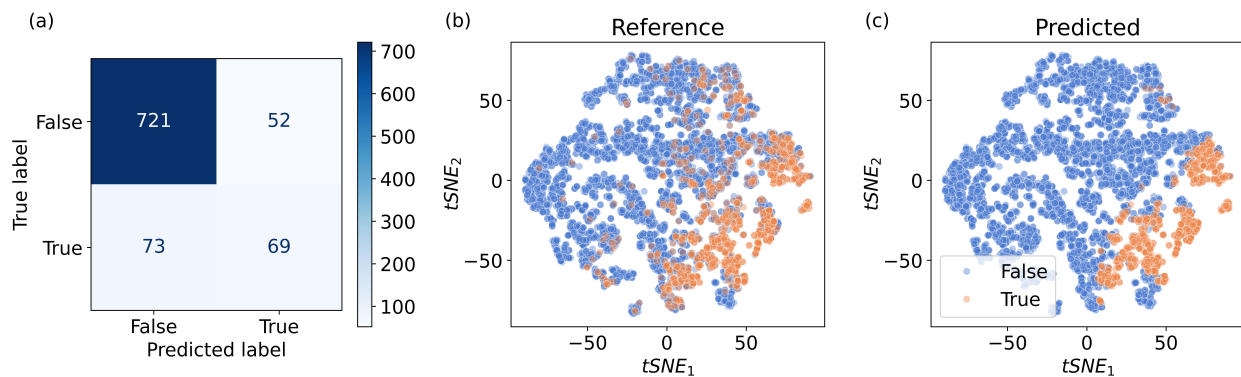


Figure 6: **Classification results of sr-mmp task from Tox21 dataset:** a) Confusion matrix of predicted labels on the test set. b) t-SNE feature representation of the entire reference dataset according to their labels. c) Feature representation of the predicted labels.

4 Discussion

One key aspect contributing to the efficacy of the eEmBERT model is its ability to capture the complex geometric attributes inherent in chemical structures, enabling accurate prediction of multiple chemical properties. Our eEmBERT-V0 model is similar to previous proven models such as MolBERT Fabian et al. [2020] or MolBART Irwin et al. [2022]. These models utilize SMILES as input data for molecular representations. However, in chemistry-related tasks, it is important to consider information about the spatial distribution of atoms within compounds. Traditional text-based (composition or SMILES formats) models are inherently limited in capturing important structural and conformational details of compounds. This limitation is a significant drawback of such models. Our eEmBERT-V1 model aims to address and mitigate this drawback. The encoding of atomic PDFs into sub-element tokens and using their corresponding



Figure 7: **Visualization of the attention scores from eEmBERT.** The top row displays the output from V0 and the bottom row the one from the V1 model.

embedding vectors as inputs to the neural network ensures a comprehensive consideration of both local atomic and global compound features. This approach is particularly significant in the context of "structure to property" tasks, where a thorough understanding of the atomic environment is crucial for accurate prediction of compound properties. As has been shown in the LA task, the V1 model excels at capturing the geometric nuances inherent in chemical structures, an observation that extends to other inorganic datasets. For instance, we can consider the visualization of the attention scores of the last layer from the V0 and V1 models. Fig. 7 demonstrates color-coded values of attention scores for materials containing Si and Osmium (Os) atoms. Notably, the V0 model assigns identical values for Si and Os atoms. In contrast, the sub-element approach divides Si and Os atoms into two (Si^0 , Si^5) and three subgroups (Os^2 , Os^4 , Os^6) respectively. Following this, the V1 model assigns diverse attention scores to individual sub-element tokens, thereby expanding the model's parameters and enhancing its predictive performance.

Despite demonstrating sufficient performance on inorganic datasets, our model shows a predictive gap compared to other models on the drug-related BACE and BBBP datasets. This discrepancy can be attributed to conformational variations among compounds present in these datasets. While we transformed SMILES into 3D structures, the existence of multiple conformers for a given SMILES formula introduces complexities. Not all conformers generated in this study may precisely match the actual structural configuration, thus diminishing the predictive power of the model. These issues may also explain the minor prediction differences observed between the V0 and V1 models in organic benchmarks. To address these issues, using accurately and thoroughly described structures could prove advantageous. Additionally, increasing the number of sub-elements may more effectively capture the complexity of chemical structures. Incorporating positional information into uniformly described databases could further enhance the predictive accuracy of our workflow. Comparative examples are provided in Appendix C. Moreover, the eEmBERT architecture supports a pre-training strategy on a large structural dataset, enabling the model to capture various chemical differences and apply this knowledge to smaller datasets.

5 Conclusions

In conclusion, the deep learning model presented in this paper signifies a marked advancement in the application of machine learning to computational chemistry. By integrating the attention mechanism and a transformer-based approach, our model can capture both local and global properties of chemical compounds, enabling highly accurate predictions of chemical properties that outperform similar approaches. The combination of principal component analysis and k-means clustering for sub-elements accounts for the nuanced effects stemming from electronic structure, a fact confirmed through the analysis of numerous chemical databases. Our classification approach, which relies on compound embeddings, results in substantially improved prediction accuracy compared to previously published scores. Additionally, t-SNE projections provide valuable insights into the classification mechanisms and can pinpoint sources of erroneous predictions. Future enhancements can likely be attained through augmentation of the sub-elements in the eEmBERT-V1 model and by the use of more sophisticated atomic descriptors.

6 Acknowledgments

The work has partially been carried out within the framework of the EUROfusion Consortium and received funding from the Euratom research and training programme by Grant Agreement No. 101052200-EUROfusion. The views and opinions expressed herein do not necessarily reflect those of the European Commission. The computational results have been obtained using the HPC infrastructure LEO of the University of Innsbruck.

7 Availability

The source code, trained weights, and example notebooks of eEmBERT available at <https://github.com/dmamur/elembert>. All data used in this paper are publicly available and can be accessed from various sources. The structure files for the

MP metallicity dataset are accessible at <https://matbench.materialsproject.org/>. The LA, SG, and DIM datasets are available at <https://github.com/sbanik2/CEGANN/tree/main/pretrained>. The BACE, BBBP, ClinTox, HIV, and SIDER datasets can be retrieved from <https://moleculenet.org/>. Structure files for the Tox21 dataset can be obtained from <https://tripod.nih.gov/tox21/challenge/data.jsp>.

Appendix A Sub-element approach

To categorize elements into sub-elements (Fig. 9), we examined various unsupervised classification algorithms, including k-means, Feature Agglomeration, neural network encoder-decoder models, and Principal Component Analysis (PCA) of PDFs combined with the k-means algorithm. The number of clusters was determined based on the oxidation states of the elements, as detailed in Table 3.

Clustering was performed using structures from the Crystallography Open Database with the scikit-learn package Pedregosa et al. [2011], with the exception of the NN encoder-decoder models. The NN architecture was manually created and symmetric, designed to reproduce the input data through a series of progressively reduced layers (Fig. 8). The central layer is configured with a number of neurons corresponding to the number of clusters. As the input atom PDF traverses the network, the model aims to identify the neuron in this central layer that produces the highest activation value. This process allows the model to determine the cluster to which the input atom is assigned.

The sub-element approach involves calculating and extracting atomic PDFs from all structures in the database. These PDFs were then aggregated according to atomic type to form the input data arrays. The models obtained from this clustering process were subsequently integrated into the eEmBERT model or could be applied as a preprocessing step. Benchmark values for different classification methods are presented in Table 4, while visual differences in predicting sub-element indices among these methods are illustrated in Fig. 10 and 11.

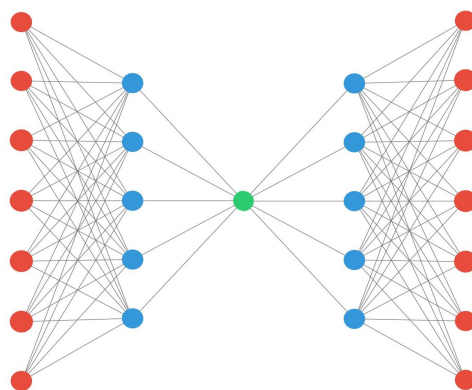


Figure 8: Neural network diagram for encoding-decoding approach.

Table 3: Cluster numbers (k) for clustering selected based on element (El) oxidation states.

N	El	k	N	El	k	N	El	k	N	El	k	N	El	k	N	El	k
1	H	3	17	Cl	9	33	As	5	49	In	4	65	Tb	4	81	Tl	3
2	He	2	18	Ar	2	34	Se	6	50	Sn	4	66	Dy	3	82	Pb	4
3	Li	2	19	K	3	35	Br	7	51	Sb	4	67	Ho	2	83	Bi	4
4	Be	3	20	Ca	3	36	Kr	2	52	Te	6	68	Er	2	84	Po	5
5	B	4	21	Sc	4	37	Rb	3	53	I	7	69	Tm	3	85	Ra	1
6	C	9	22	Ti	5	38	Sr	3	54	Xe	5	70	Yb	3	86	Ac	3
7	N	9	23	V	7	39	Y	4	55	Cs	3	71	Lu	2	87	Th	4
8	O	5	24	Cr	9	40	Zr	5	56	Ba	2	72	Hf	4	88	Pa	5
9	F	2	25	Mn	11	41	Nb	6	57	La	3	73	Ta	6	89	U	6
10	Ne	2	26	Fe	9	42	Mo	9	58	Ce	4	74	W	9	90	Np	6
11	Na	3	27	Co	7	43	Tc	10	59	Pr	4	75	Re	10	91	Pu	7
12	Mg	3	28	Ni	6	44	Ru	10	60	Nd	3	76	Os	10	92	Am	6
13	Al	4	29	Cu	5	45	Rh	8	61	Pm	2	77	Ir	11	93	Cm	3
14	Si	9	30	Zn	3	46	Pd	3	62	Sm	3	78	Pt	5	94	Bk	1
15	P	9	31	Ga	4	47	Ag	5	63	Eu	3	79	Au	6	95	Cf	1
16	S	9	32	Ge	6	48	Cd	3	64	Gd	4	80	Hg	4	96	Rn	1

Appendix B Organic benchmarks

B.1 BACE Dataset

The BACE dataset includes 1,513 compounds classified as active or inactive inhibitors of the β -secretase enzyme, associated with Alzheimer’s disease. Fig. 12 shows the eEmBERT-V1 predictions, revealing two clusters with intermingled labels, which lead to some misclassifications.

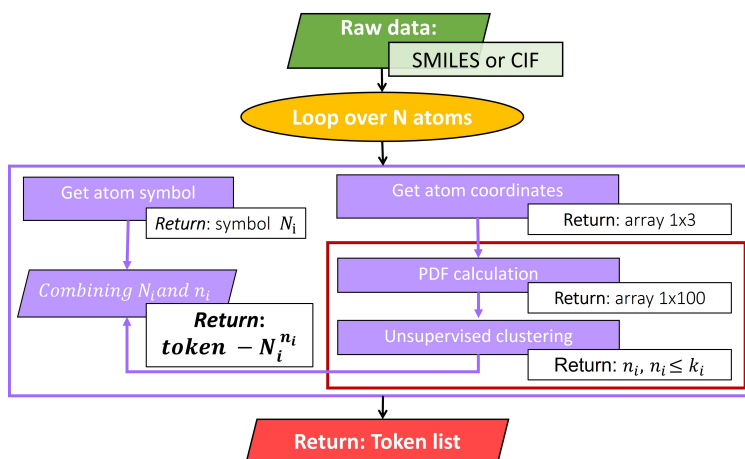


Figure 9: **Workflow of the unsupervised classification module.** The process starts with compounds provided in Crystallographic Information File (CIF) or SMILES format as input data. The module first extracts the atomic symbols and Cartesian coordinates of all atoms from this input. Next, PDFs are computed based on these coordinates. The computed PDFs are then subjected to unsupervised clustering. The resulting clusters are mapped to the atomic symbols, facilitating their conversion into tokens for further analysis.

Table 4: Performance of different classification models applied to datasets used in this work.

Benchmark	Km	NN	FA	PCA
MP metallicity	0.967	0.969	0.967	0.967
SG	0.954	0.954	0.953	0.967
LA	0.987	0.988	0.988	0.987
DIM	0.881	0.948	0.950	0.932
BACE	0.871	0.856	0.817	0.845
BBBP	0.887	0.893	0.924	0.896
ClinTox	0.973	0.969	0.970	0.967
HIV	0.978	0.979	0.977	0.977

B.2 BBBP Dataset

The BBBP dataset contains 2,039 compounds, categorized by their ability to penetrate the blood-brain barrier. Fig. 13 shows the confusion matrix and t-SNE plots, illustrating label separation.

B.3 ClinTox Dataset

Containing 1,491 compounds, the ClinTox dataset assesses clinical toxicity and FDA approval status. Fig. 14 shows the results. Due to the low number of negative instances, the model accurately predicts all negative values in a small region and only for the training set.

B.4 HIV Dataset

The HIV dataset, which includes approximately 41,000 data points with 1,443 positives, is used to predict patient treatment responses and drug resistance. Fig. 15 highlights the points that lead to errors and decrease the efficiency of the classification.

B.5 SIDER Dataset

The SIDER dataset serves as a comprehensive pharmacovigilance resource, containing structured information on drug-associated side effects. Curated from diverse sources such as clinical trials, regulatory reports, and medical literature, it offers a systematic compilation of adverse drug reactions associated with various pharmaceutical interventions. The training results are presented in Table 5. Fig. 16 illustrates label separation in the feature space for the SIDER-1 task.

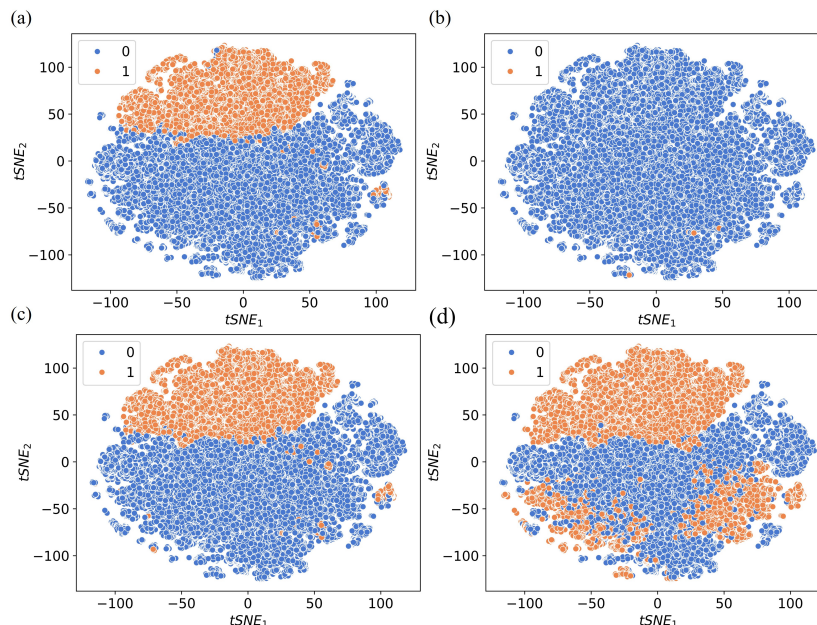


Figure 10: **Sub-element classification of Lithium atoms.** t-SNE Plots for Mg for k-means (a), Feature Agglomeration (b), NN encoder-decoder (c) and PCA-k-means (d) algorithms.

Table 5: ROC-AUC performances of V0 and V1 models on the SIDER dataset. MMGNN denotes the prior top-performing results.

SIDER N	1	2	3	4	5	6	7	8	9
V0	0.684	0.709	0.985	0.676	0.847	0.738	0.945	0.839	0.739
V1	0.663	0.707	0.983	0.689	0.838	0.744	0.941	0.832	0.724
MMGNN	0.754	0.693	0.723	0.744	0.817	0.741	-	-	-
SIDER N	10	11	12	13	14	15	16	17	18
V0	0.775	0.908	0.819	0.853	0.809	0.723	0.926	0.822	0.724
V1	0.760	0.892	0.816	0.849	0.782	0.737	0.917	0.833	0.736
MMGNN	-	-	-	-	-	-	-	-	-
SIDER N	19	20	21	22	23	24	25	26	27
V0	0.724	0.759	0.764	0.700	0.927	0.598	0.747	0.925	0.698
V1	0.736	0.772	0.726	0.708	0.923	0.599	0.742	0.916	0.684
MMGNN	-	-	-	-	-	-	-	-	-

Appendix C Position encoding

The order of atoms in structures could sometimes be important, especially if a set of structures was generated or described in the same way. If the input sequence follows specific rules and order, positional encoding can capture additional information and enhance prediction quality. Comparing our property predictions with and without positional embeddings, we find that the former indeed enhances the accuracy of the predictions. The results are outlined in Table 6.

Table 6: ROC-AUC values for the V1 model with (P^+) and without positional encoding (P^-).

BENCHMARK	P^+	P^-
MP METALLICITY	0.965	0.966
SG	0.968	0.966
LA	0.980	0.969
DIM	0.958	0.958
BACE	0.856	0.808
BBBP	0.905	0.888
ClinTox	0.951	0.946
HIV	0.979	0.980

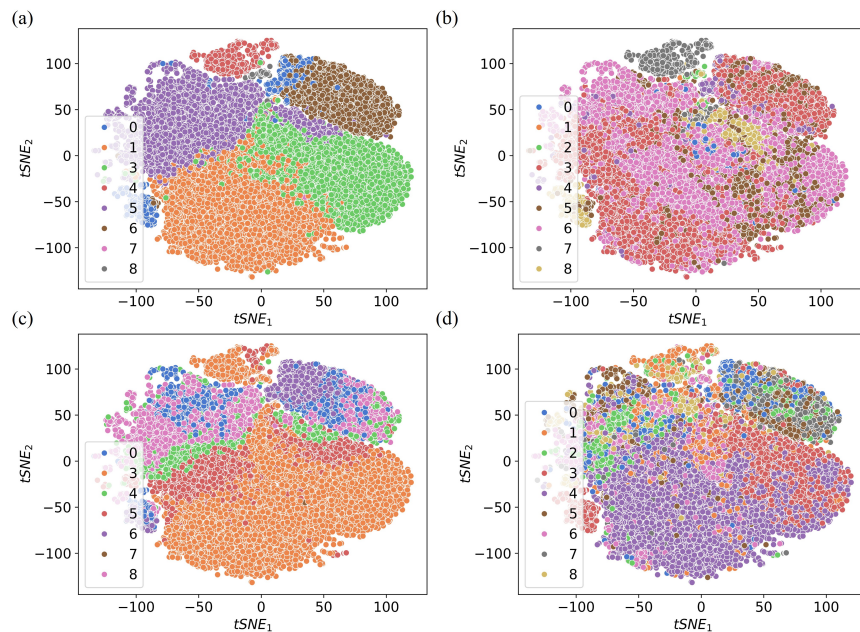


Figure 11: **Sub-element classification of Chlorine atoms.** t-SNE Plots for Li for k-means (a), Feature Agglomeration (b), NN encoder-decoder (c), and PCA- k-means (d) algorithms.

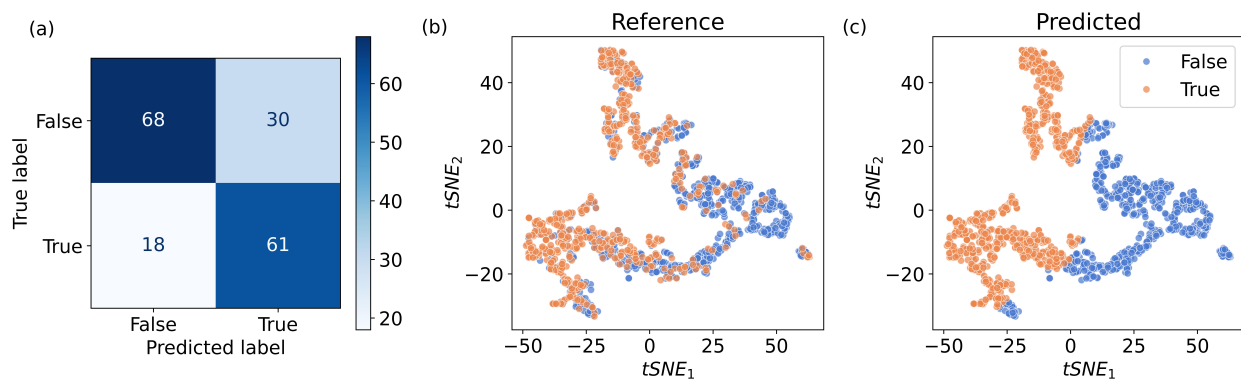


Figure 12: **Classification of BACE data:** a) Confusion matrix of predicted labels on the test set. b) t-SNE feature representation of the entire reference dataset according to their labels. c) Feature representation of the predicted labels.

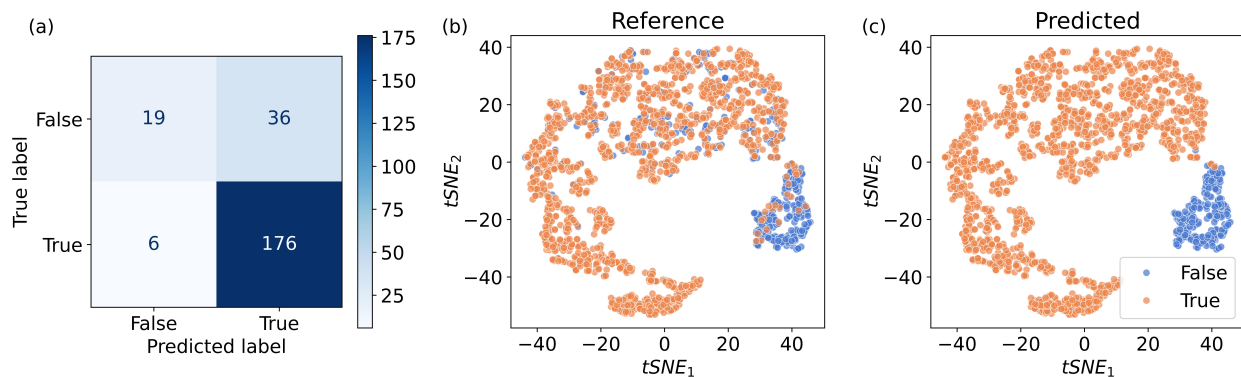


Figure 13: **Classification of BBBP data:** a) Confusion matrix of predicted labels on the test set. b) t-SNE feature representation of the entire reference dataset according to their labels. c) Feature representation of the predicted labels.

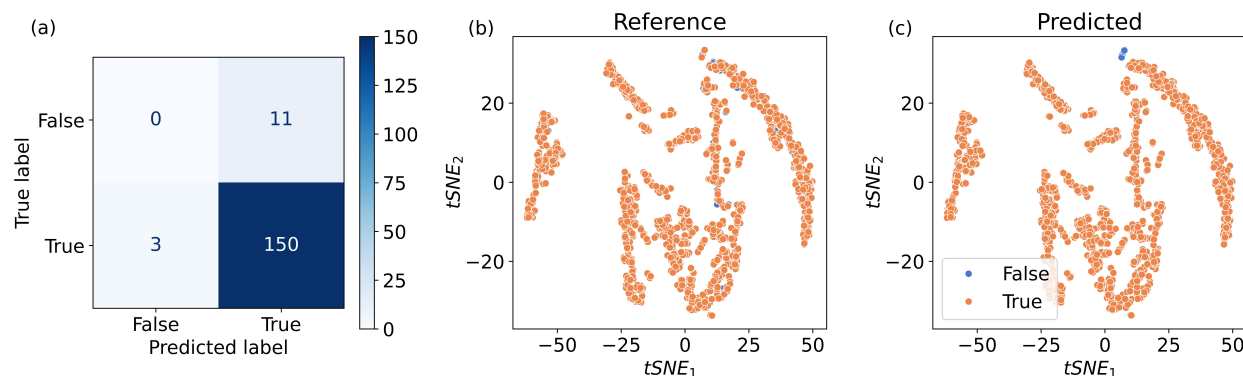


Figure 14: **Classification of ClinTox FDA approval task:** a) The confusion matrix of predicted labels on the test set. b) The t-SNE feature representation of the entire reference dataset according to their labels. c) The feature representation of the predicted labels.

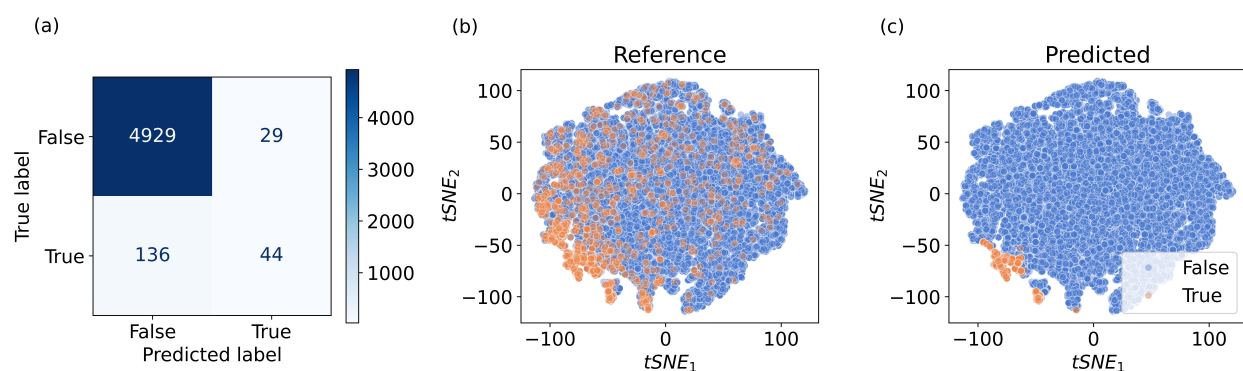


Figure 15: **Classification of HIV data:** a) Confusion matrix of predicted labels on the test set. b) t-SNE feature representation of the entire reference dataset according to their labels. c) Feature representation of the predicted labels.

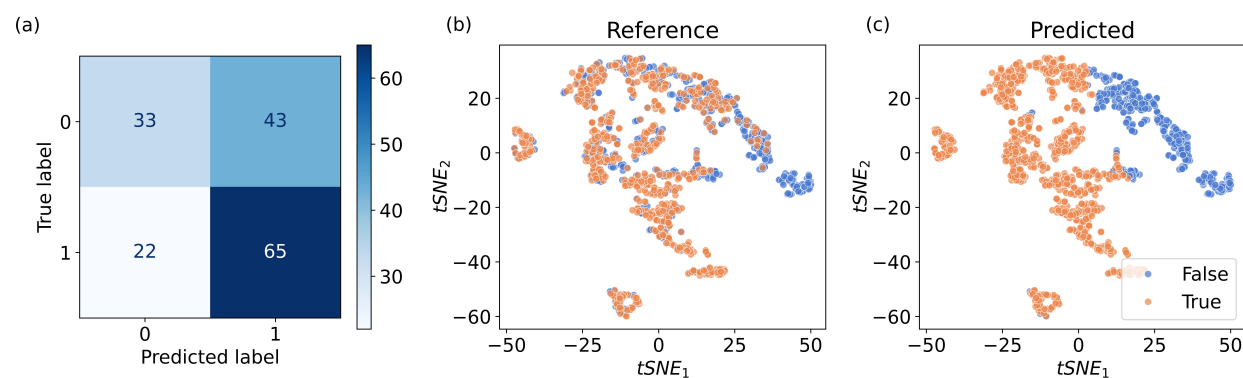


Figure 16: **Classification of SIDER-1 task:** a) Confusion matrix of predicted labels on the test set. b) t-SNE feature representation of the entire reference dataset according to their labels. c) Feature representation of the predicted labels.

References

- Man-Fai Ng, Jin Zhao, Qingyu Yan, Gareth J Conduit, and Zhi Wei Seh. Predicting the state of charge and health of batteries using data-driven machine learning. *Nature Machine Intelligence*, 2(3):161–170, 2020. ISSN 2522-5839. doi:10.1038/s42256-020-0156-7.
- Yue Liu, Biru Guo, Xinxin Zou, Yajie Li, and Siqi Shi. Machine learning assisted materials design and discovery for rechargeable batteries. *Energy Storage Materials*, 31:434–450, 2020. ISSN 2405-8297. doi:10.1016/j.ensm.2020.06.033.
- Vaishali Sawant, Rashmi Deshmukh, and Chetan Awati. Machine learning techniques for prediction of capacitance and remaining useful life of supercapacitors: A comprehensive review. *Journal of Energy Chemistry*, 77:438–451, 2023. ISSN 2095-4956. doi:10.1016/j.jechem.2022.11.012.
- Yuma Iwasaki, Ichiro Takeuchi, Valentin Stanev, Aaron Gilad Kusne, Masahiko Ishida, Akihiro Kirihiro, Kazuki Ihara, Ryohto Sawada, Koichi Terashima, Hiroko Someya, Ken ichi Uchida, Eiji Saitoh, and Shinichi Yorozu. Machine-learning guided discovery of a new thermoelectric material. *Scientific Reports*, 9(1):1–7, 2019. ISSN 20452322. doi:10.1038/s41598-019-39278-z.
- Muhammad Naveed Akhter, Saad Mekhilef, Hazlie Mokhlis, and Noraisyah Mohamed Shah. Review on forecasting of photovoltaic power generation based on machine learning and metaheuristic techniques. *IET Renewable Power Generation*, 13(7):1009–1023, 2019. ISSN 17521424. doi:10.1049/iet-rpg.2018.5649.
- Takashi Toyao, Zen Maeno, Satoru Takakusagi, Takashi Kamachi, Ichigaku Takigawa, and Ken-ichi Shimizu. Machine learning for catalysis informatics: Recent applications and prospects. *ACS Catalysis*, 10(3):2260–2297, 2 2020. doi:10.1021/acscatal.9b04186.
- Jessica Vamathevan, Dominic Clark, Paul Czodrowski, Ian Dunham, Edgardo Ferran, George Lee, Bin Li, Anant Madabhushi, Parantu Shah, Michaela Spitzer, and Shanrong Zhao. Applications of machine learning in drug discovery and development. *Nature Reviews Drug Discovery*, 18(6):463–477, 2019. ISSN 14741784. doi:10.1038/s41573-019-0024-5.
- Tomas Mikolov, Kai Chen, Greg Corrado, and Jeffrey Dean. Efficient estimation of word representations in vector space. 2013. doi:10.48550/arXiv.1301.3781.
- Vahe Tshitoyan, John Dagdelen, Leigh Weston, Alexander Dunn, Ziqin Rong, Olga Kononova, Kristin A. Persson, Gerbrand Ceder, and Anubhav Jain. Unsupervised word embeddings capture latent knowledge from materials science literature. *Nature*, 571(7763):95–98, 2019. ISSN 14764687. doi:10.1038/s41586-019-1335-8.
- Katja Hansen, Franziska Biegler, Raghunathan Ramakrishnan, Wiktor Pronobis, O. Anatole Von Lilienfeld, Klaus Robert Müller, and Alexandre Tkatchenko. Machine learning predictions of molecular properties: Accurate many-body potentials and nonlocality in chemical space. *Journal of Physical Chemistry Letters*, 6(12):2326–2331, 2015. ISSN 19487185. doi:10.1021/acs.jpcclett.5b00831.
- Sabrina Jaeger, Simone Fulle, and Samo Turk. Mol2vec: Unsupervised machine learning approach with chemical intuition. *Journal of Chemical Information and Modeling*, 58(1):27–35, 2018. ISSN 15205142. doi:10.1021/acs.jcim.7b00616.
- Garrett B. Goh, Nathan O. Hodas, Charles Siegel, and Abhinav Vishnu. Smiles2vec: An interpretable general-purpose deep neural network for predicting chemical properties. 2018. doi:10.48550/arXiv.1712.02034.
- Yu Fang Zhang, Xiangeng Wang, Aman Chandra Kaushik, Yanyi Chu, Xiaoqi Shan, Ming Zhu Zhao, Qin Xu, and Dong Qing Wei. Spvec: A word2vec-inspired feature representation method for drug-target interaction prediction. *Frontiers in Chemistry*, 7(January):1–11, 2020a. ISSN 22962646. doi:10.3389/fchem.2019.00895.
- Valentin Stanev, Corey Oses, A. Gilad Kusne, Efrain Rodriguez, Johnpierre Paglione, Stefano Curtarolo, and Ichiro Takeuchi. Machine learning modeling of superconducting critical temperature. *npj Computational Materials*, 4(1), 2018. ISSN 20573960. doi:10.1038/s41524-018-0085-8.
- Chi Chen, Weike Ye, Yunxing Zuo, Chen Zheng, and Shyue Ping Ong. Graph networks as a universal machine learning framework for molecules and crystals. *Chemistry of Materials*, 31(9):3564–3572, 5 2019. ISSN 15205002. doi:10.1021/acs.chemmater.9b01294.
- Shufeng Kong, Francesco Ricci, Dan Guevarra, Jeffrey B. Neaton, Carla P. Gomes, and John M. Gregoire. Density of states prediction for materials discovery via contrastive learning from probabilistic embeddings. *Nature Communications*, 13(1):1–12, 2022. ISSN 20411723. doi:10.1038/s41467-022-28543-x.
- Marco Gori, Gabriele Monfardini, and Franco Scarselli. A new model for learning in graph domains. *Proceedings of the International Joint Conference on Neural Networks*, 2:729–734, 2005. doi:10.1109/IJCNN.2005.1555942.

- Shuo Zhang, Yang Liu, and Lei Xie. Molecular mechanics-driven graph neural network with multiplex graph for molecular structures. *arXiv*, pages 1–14, 2020b. doi:10.48550/arXiv.2011.07457.
- Zeren Shui and George Karypis. Heterogeneous molecular graph neural networks for predicting molecule properties. *Proceedings - IEEE International Conference on Data Mining, ICDM*, 2020-Novem:492–500, 2020. ISSN 15504786. doi:10.1109/ICDM50108.2020.00058.
- Victor Fung, Jiaxin Zhang, Eric Juarez, and Bobby G. Sumpter. Benchmarking graph neural networks for materials chemistry. *npj Computational Materials*, 7(1):1–8, 2021. ISSN 20573960. doi:10.1038/s41524-021-00554-0.
- Tian Xie and Jeffrey C. Grossman. Crystal graph convolutional neural networks for an accurate and interpretable prediction of material properties. *Physical Review Letters*, 120(14):145301, 4 2018. ISSN 10797114. doi:10.1103/PhysRevLett.120.145301.
- Zhichun Guo, Chuxu Zhang, Wenhao Yu, John Herr, Olaf Wiest, Meng Jiang, and V. Nitesh Chawla. Few-shot graph learning for molecular property prediction. *The Web Conference 2021 - Proceedings of the World Wide Web Conference, WWW 2021*, pages 2559–2567, 2021. doi:10.1145/3442381.3450112.
- Albert P. Bartók, Risi Kondor, and Gábor Csányi. On representing chemical environments. *Physical Review B - Condensed Matter and Materials Physics*, 87(18):1–16, 2013. ISSN 10980121. doi:10.1103/PhysRevB.87.184115.
- Haoyan Huo and Matthias Rupp. Unified representation of molecules and crystals for machine learning. *Machine Learning: Science and Technology*, 3:045017, 2022. ISSN 26322153. doi:10.1088/2632-2153/aca005.
- Jörg Behler. Four generations of high-dimensional neural network potentials. *Chemical Reviews*, 121:10037–10072, 2021. ISSN 15206890. doi:10.1021/acs.chemrev.0c00868.
- Oliver T. Unke and Markus Meuwly. Physnet: A neural network for predicting energies, forces, dipole moments, and partial charges. *Journal of Chemical Theory and Computation*, 15(6):3678–3693, 2019. ISSN 15499626. doi:10.1021/acs.jctc.9b00181.
- Ashish Vaswani, Noam Shazeer, Niki Parmar, Jakob Uszkoreit, Llion Jones, Aidan N. Gomez, Lukasz Kaiser, and Illia Polosukhin. Attention is all you need. 2023. doi:10.48550/arXiv.1712.02034.
- Steph Yves Louis, Yong Zhao, Alireza Nasiri, Xiran Wang, Yuqi Song, Fei Liu, and Jianjun Hu. Graph convolutional neural networks with global attention for improved materials property prediction. *Physical Chemistry Chemical Physics*, 22(32):18141–18148, 2020. ISSN 14639076. doi:10.1039/d0cp01474e.
- Simon J.L. Billinge. The rise of the x-ray atomic pair distribution function method: A series of fortunate events. *Philosophical Transactions of the Royal Society A: Mathematical, Physical and Engineering Sciences*, 377(2147), 2019. ISSN 1364503X. doi:10.1098/rsta.018.0413.
- Ask Hjorth Larsen, Jens Jørgen Mortensen, Jakob Blomqvist, Ivano E Castelli, Rune Christensen, Marcin Dułak, Jesper Friis, Michael N Groves, Bjørk Hammer, Cory Hargus, Eric D Hermes, Paul C Jennings, Peter Bjerre Jensen, James Kermode, John R Kitchin, Esben Leonhard Kolsbjerg, Joseph Kubal, Kristen Kaasbjerg, Steen Lysgaard, Jón Bergmann Maronsson, Tristan Maxson, Thomas Olsen, Lars Pastewka, Andrew Peterson, Carsten Rostgaard, Jakob Schiøtz, Ole Schütt, Mikkel Strange, Kristian S Thygesen, Tejs Vegge, Lasse Vilhelmsen, Michael Walter, Zhenhua Zeng, and Karsten W Jacobsen. The atomic simulation environment—a python library for working with atoms. *Journal of Physics: Condensed Matter*, 29(27):273002, 2017. ISSN 0953-8984. doi:10.1088/1361-648X/aa680e.
- Shokirbek Shermukhamedov, Dilorom Mamurjonova, and Michael Probst. Structure to property: Chemical element embeddings and a deep learning approach for accurate prediction of chemical properties. *J. Chem. Inf. Model.*, 64(16):5762–5770, 2024. doi:10.1021/acs.jcim.3c01990.
- Wolfgang Damm, Antonio Frontera, Julian Tirado Rives, and William L Jorgensen. Opls all-atom force field for carbohydrates. *Journal of computational chemistry*, 18(16):1955–1970, 1997. doi:10.1002/(SICI)1096-987X(199712)18:16<1955::AID-JCC1>3.0.CO;2-L.
- Saulius Gražulis, Daniel Chateigner, Robert T Downs, A F T Yokochi, Miguel Quirós, Luca Lutterotti, Elena Manakova, Justas Butkus, Peter Moeck, and Armel Le Bail. Crystallography open database – an open-access collection of crystal structures. *Journal of Applied Crystallography*, 42(4):726–729, 8 2009. doi:10.1107/S0021889809016690.
- Saulius Gražulis, Adriana Daškevič, Andrius Merkys, Daniel Chateigner, Luca Lutterotti, Miguel Quirós, Nadezhda R Serebryanaya, Peter Moeck, Robert T Downs, and Armel Le Bail. Crystallography open database (cod): an open-access collection of crystal structures and platform for world-wide collaboration. *Nucleic Acids Research*, 40(D1):D420–D427, 1 2012. ISSN 0305-1048. doi:10.1093/nar/gkr900.
- Anubhav Jain, Shyue Ping Ong, Geoffroy Hautier, Wei Chen, William Davidson Richards, Stephen Dacek, Shreyas Cholia, Dan Gunter, David Skinner, Gerbrand Ceder, and Kristin A. Persson. Commentary: The materials project: A materials genome approach to accelerating materials innovation. *APL Materials*, 1(1), 2013. ISSN 2166532X. doi:10.1063/1.4812323.

- Shyue Ping Ong, Shreyas Cholia, Anubhav Jain, Miriam Brafman, Dan Gunter, Gerbrand Ceder, and Kristin A. Persson. The materials application programming interface (api): A simple, flexible and efficient api for materials data based on representational state transfer (rest) principles. *Computational Materials Science*, 97:209–215, 2015. ISSN 09270256. doi:10.1016/j.commatsci.2014.10.037.
- Suvo Banik, Debdas Dhabal, Henry Chan, Sukriti Manna, Mathew Cherukara, Valeria Molinero, and Subramanian K.R.S. Sankaranarayanan. Cegann: Crystal edge graph attention neural network for multiscale classification of materials environment. *npj Computational Materials*, 9(1):1–12, 2023. ISSN 20573960. doi:10.1038/s41524-023-00975-z.
- Angelo Ziletti, Devinder Kumar, Matthias Scheffler, and Luca M. Ghiringhelli. Insightful classification of crystal structures using deep learning. *Nature Communications*, 9(1):1–10, 2018. ISSN 20411723. doi:10.1038/s41467-018-05169-6.
- Zhenqin Wu, Bharath Ramsundar, Evan N. Feinberg, Joseph Gomes, Caleb Geniesse, Aneesh S. Pappu, Karl Leswing, and Vijay Pande. Moleculenet: A benchmark for molecular machine learning. *Chemical Science*, 9(2):513–530, 2018. ISSN 20416539. doi:10.1039/c7sc02664a.
- Michael Kuhn, Ivica Letunic, Lars Juhl Jensen, and Peer Bork. The sider database of drugs and side effects. *Nucleic Acids Research*, 44(D1):D1075–D1079, 2016. ISSN 13624962. doi:10.1093/nar/gkv1075.
- Noel M O’Boyle, Michael Banck, Craig A James, Chris Morley, Tim Vandermeersch, and Geoffrey R Hutchison. Open babel: An open chemical toolbox. *Journal of Cheminformatics*, 3(33):1–14, 2011. ISSN 17582946. doi:10.1186/1758-2946-3-33.
- Rdkit: Open-source cheminformatics. URL <https://www.rdkit.org>.
- François Chollet et al. Keras. 2015. URL <https://keras.io>.
- Chi Chen and Shyue Ping Ong. Atomsets as a hierarchical transfer learning framework for small and large materials datasets. *npj Computational Materials*, 7(1), 2021. ISSN 20573960. doi:10.1038/s41524-021-00639-w.
- Yuquan Li, Chang-Yu Hsieh, Ruiqiang Lu, Xiaoqing Gong, Xiaorui Wang, Pengyong Li, Shuo Liu, Yanan Tian, Dejun Jiang, Jiaxian Yan, Qifeng Bai, Huanxiang Liu, Shengyu Zhang, and Xiaojun Yao. Glam : An adaptive graph learning method for automated molecular interactions and properties predictions. *Nature Machine Intelligence*, 4(7):645–651, 2022. ISSN 2522-5839. doi:10.1038/s42256-022-00501-8.
- Pengyong Li, Yuquan Li, Chang-Yu Hsieh, Shengyu Zhang, Xianggen Liu, Huanxiang Liu, Sen Song, and Xiaojun Yao. Trimnet: learning molecular representation from triplet messages for biomedicine. *Briefings in Bioinformatics*, 22(4): bbaa266, 7 2021. ISSN 1477-4054. doi:10.1093/bib/bbaa266.
- Jinheon Baek, Minki Kang, and Sung Ju Hwang. Accurate learning of graph representations with graph multiset pooling. 2021. doi:10.48550/arXiv.2102.11533.
- Benedek Fabian, Thomas Edlich, H el ena Gaspar, Marwin Segler, Joshua Meyers, Marco Fiscato, and Mohamed Ahmed. Molecular representation learning with language models and domain-relevant auxiliary tasks. 2020. doi:10.48550/arXiv.2011.13230.
- Ross Irwin, Spyridon Dimitriadis, Jiazhen He, and Esben Jannik Bjerrum. Chemformer: A pre-trained transformer for computational chemistry. *Machine Learning: Science and Technology*, 3(1), 2022. ISSN 26322153. doi:10.1088/2632-2153/ac3ffb.
- Fabian Pedregosa, Ga el Varoquaux, Alexandre Gramfort, Vincent Michel, Bertrand Thirion, Olivier Grisel, Mathieu Blondel, Peter Prettenhofer, Ron Weiss, Vincent Dubourg, Jake Vanderplas, Alexandre Passos, David Cournapeau, Matthieu Brucher, Matthieu Perrot, and  douard Duchesnay. Scikit-learn: Machine learning in python. *Journal of Machine Learning Research*, 12(85):2825–2830, 2011. URL <http://jmlr.org/papers/v12/pedregosa11a.html>.